Multiwavelength Study of a Solar Eruption from AR NOAA 11112: II. Large-Scale Coronal Wave and Loop Oscillation

Pankaj Kumar · K.-S. Cho · P.F. Chen · S.-C. Bong · Sung-Hong Park

Abstract We analyze multiwavelength observations of an M2.9/1N flare that occurred in AR NOAA 11112 on 16 October 2010. AIA 211 Å EUV images reveal the presence of a faster coronal wave (decelerating from ≈ 1390 to ≈ 830 km s^{-1}) propagating ahead of a slower wave (decelerating from ≈ 416 to ≈ 166 km s^{-1}) towards the western limb. The dynamic radio spectrum from Sagamore Hill radio telescope shows the presence of a metric type II radio burst, which reveals the presence of a coronal shock wave (speed ≈ 800 km s^{-1}). The speed of the faster coronal wave, derived from AIA 211 Å images, is found to be comparable to the coronal shock speed. AIA 171 Å high-cadence observations showed that a coronal loop, which was located at a distance of $\approx 0.32 R_{\odot}$ to the west of the flaring region, started to oscillate by the end of the impulsive phase of the flare. The results indicate that the faster coronal wave may be the first driver of the transversal oscillations of coronal loop. As the slower wave passed through the coronal loop, the oscillations became even stronger. There was a plasmoid eruption observed in EUV and a white-light CME was recorded, having velocity of ≈ 340–350 km s^{-1}. STEREO 195 Å images show an EIT wave, propagating in the same direction as the lower-speed coronal wave observed in AIA, but decelerating from ≈ 320 to ≈ 254 km s^{-1}. These observations reveal the co-existence of both waves (*i.e.* coronal Moreton and EIT waves), and the type II radio burst seems to be associated with the coronal Moreton wave.

P. Kumar (✉) · K.-S. Cho · S.-C. Bong · S.-H. Park
Korea Astronomy and Space Science Institute (KASI), Daejeon 305-348, Republic of Korea
e-mail: pankaj@kasi.re.kr

K.-S. Cho
NASA Goddard Space Flight Center, Greenbelt, MD, USA

K.-S. Cho
Department of Physics, The Catholic University of America, Washington, DC, USA

P.F. Chen
School of Astronomy and Space Science, Nanjing University, Nanjing 210093, China

1. Introduction

Large-scale coronal waves are often observed during solar eruptions. For example, the so-called EIT waves are transient wavelike disturbances in the solar corona that propagate with the typical speed of $170 - 350$ km s^{-1} followed by the expanding coronal dimming (Thompson *et al.*, 1998, 1999; Klassen *et al.*, 2000). These were first observed by the *EUV imaging Telescope* (EIT) onboard SOHO (Delaboudinière *et al.*, 1995). It is now widely accepted that EIT waves are associated with coronal mass ejections (CMEs) rather than solar flares (Delannée and Aulanier, 1999; Biesecker *et al.*, 2002; Cliver *et al.*, 2005; Chen, 2006). Regarding the spatial relationship between EIT waves and CMEs, some authors found that they are cospatial (Chen, 2009; Dai *et al.*, 2010), whereas some others claimed that EIT wave fronts are ahead of the CME leading edge (Veronig, Temmer, and Vršnak, 2008; Patsourakos *et al.*, 2009; Patsourakos and Vourlidas, 2009; Kienreich, Temmer, and Veronig, 2009; Kienreich *et al.*, 2011; Veronig *et al.*, 2010; Muhr *et al.*, 2011). EIT waves were usually explained as the fast-mode magnetoacoustic waves in the corona (*e.g.*, Wang, 2000; Wu *et al.*, 2001); therefore, they would be coronal counterparts of the Hα Moreton waves that are observed in the chromosphere with a velocity of $\approx 500 - 2000$ km s^{-1} (Moreton and Ramsey, 1960). The fast-mode wave model was first questioned by Delannée and Aulanier (1999). Furthermore, Eto *et al.* (2002) investigated CME-related waves in an X-class flare event and found that an EIT wave front is not cospatial with the Moreton wave front inferred from filament winking, and the propagation speeds of both waves were clearly different. Therefore, several non-wave models were later developed (see Wills-Davey and Attrill, 2009; Warmuth, 2010; Gallagher and Long, 2011; Chen, 2011; Zhukov, 2011 for reviews). On the basis of MHD numerical simulation, Chen *et al.* (2002) proposed that EIT waves are apparently moving brightenings, which are generated by successive stretching of the closed field lines pushed by an erupting flux rope. According to the field-line stretching model (Chen *et al.*, 2002; Chen, Fang, and Shibata, 2005), a fast-mode magnetoacoustic wave (or coronal Moreton wave) should be ahead of the EIT wave in a CME event, which was confirmed by Harra and Sterling (2003). Recently, using high-resolution SDO/AIA observations, Chen and Wu (2011) convincingly reported the existence of the fast-mode coronal Moreton wave (*i.e.* coronal counterpart of Moreton wave), which is three times faster than the EIT wave.

Whereas EIT waves show a good correlation with the decimetric–metric type II radio bursts, the speed derived from the type II radio burst is usually three times larger than the EIT wave speed (Klassen *et al.*, 2000). The speed of a Moreton wave, however, matches with the speed derived from type II radio bursts (Eto *et al.*, 2002; Warmuth *et al.*, 2004b). This suggests that the Moreton wave, rather than the EIT wave, and the type II radio burst are two aspects of a single phenomenon, an MHD fast-mode shock propagating in the corona (Uchida, 1974). However, it was also claimed that there is a significant fraction of events where EIT waves are found to be a coronal signature directly associated with Moreton waves, *i.e.*, both are cospatial (Warmuth *et al.*, 2001, 2004b; Warmuth, Mann, and Aurass, 2005; Vršnak *et al.*, 2002; Veronig *et al.*, 2006; Muhr *et al.*, 2010).

Besides the debates on EIT waves, the origin of coronal shock waves (usually evident in the form of type II radio burst) is also under debate (for details see Warmuth, 2007; Chen and Fang, 2011). They may be driven by two possible physical mechanisms, *i.e.*

i) a blast wave ignited by the pressure pulse of a flare (Vršnak *et al.*, 1995; Vršnak and Lulić, 2000a, 2000b; Khan and Aurass, 2002; Narukage *et al.*, 2002; Hudson *et al.*, 2003; Magdalenić *et al.*, 2010),

ii) a piston-driven shock due to a CME (Klassen *et al.*, 1999; Klassen, Pohjolainen, and Klein, 2003; Cho *et al.*, 2011).

Thus, coronal shock waves may be associated with solar flares, CMEs, or some combination of these phenomena (Magara *et al.*, 2000; Magdalenić *et al.*, 2008; Vršnak and Cliver, 2008).

In this paper, we analyze the multiwavelength observations from SDO/AIA and STEREO to investigate the a large-scale coronal wave event and its impact on the solar corona in terms of loop oscillations. In Section 2, we will present multiwavelength observations of the large-scale coronal waves and the CME. In the last section, we will discuss the results and draw conclusions.

2. Observations

The *Atmospheric Imaging Assembly* (AIA: Lemen *et al.*, 2012) on board the *Solar Dynamics Observatory* (SDO: Pesnell, Thompson, and Chamberlin, 2012) mission provides multiwavelength high-resolution full-disk images of the corona and transition region. The field of view of each image is $1.3 R_\odot$. The pixel size of the images is $0.6''$ and the cadence is 12 s. We use AIA 171, 211 and 193 Å EUV observations to investigate the evolution of coronal waves associated with an M2.9 flare that occurred in AR NOAA 11112 on 16 October 2010. The detailed description of flare energy build up and triggering mechanism has been discussed in Kumar *et al.* (2012) (hereafter Paper I). This paper consists of the description of flare/CME associated coronal waves kinematics as well as the interaction of these waves with the coronal loop, which showed transverse oscillations while the waves were passing through.

2.1. Coronal Waves

Figure 1 displays SDO/AIA 171 Å EUV image overlaid by SDO/HMI (Schou *et al.*, 2012) magnetogram contours to show the magnetic environment in a larger field of view. Red/blue represents a positive/negative polarity field region. We can see a huge filament lying along the polarity inversion line (PIL), which did not erupt during the flare. The flare site is indicated by an arrow. A small loop system, indicated by another arrow, was located $\approx 0.32 R_\odot$ away from the flare site on its west side. Aschwanden and Schrijver (2011) have extensively studied the properties of the transversal oscillations of this loop system. They have interpreted it as kink mode transversal oscillations and studied the properties of the MHD modes and diagnosed the local plasma conditions of the oscillating loop system. In particular, they noticed that, unlike most previously studied events, the oscillation of this coronal loop showed no damping for several periods.

In this paper, we only investigate the most probable driver of loop oscillations under the baseline of multiwavelength observations of the M-class flare and the associated large-scale wave phenomena. We use base-difference images to reduce the artifacts and for the correct information regarding the waves (Attrill, 2010). For investigating the driver of loop oscillations, we make AIA 211 Å base-difference images. The selected base-difference images are displayed in Figure 2. AIA 211 Å EUV images are sensitive to the temperature of 2 MK. The '+' symbol marks the location of the small coronal loop in each image. The first image at
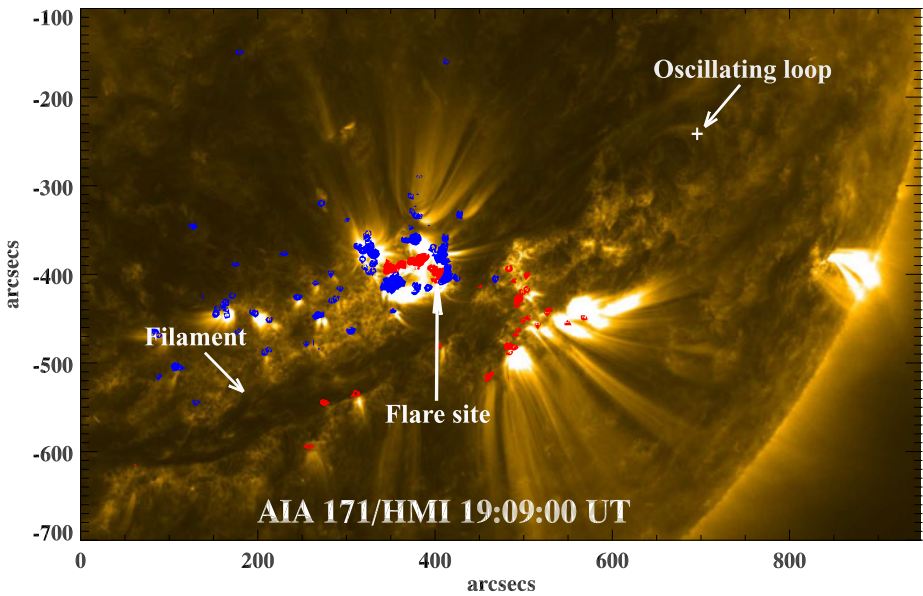
Figure 1 SDO/AIA 171 Å image overlaid by HMI magnetogram contours (red is for positive, blue for negative polarity) showing a huge filament system lying along the polarity inversion line, and the sites of the flare and the oscillating loop system. The loop apex is marked by the '+' symbol.

19:10:48 UT shows the flare site as well as the extended bright flare ribbon towards the west direction. We can see the propagating disturbance/wave towards the west along the direction of bright ribbons (19:11:36 UT). Coronal dimmings were observed behind the propagating wavefront probably due to the depletion in plasma density. At 19:14:00 UT, the nearly circular shape of the fast wavefront is evident in the image, which is indicated by the arrows and marked by 'F'. At this time it approached the site of the coronal loop system indicated by the '+' symbol (shown in the 171 Å image, Figure 1), which started to oscillate. The 'F' front continued to expand towards the west in a ballooning shape and it could be tracked nearly up to the western limb (shown by arrows at 19:16:24 UT). In the meanwhile, we see another bright wavefront at 19:16:24 UT behind the faster front, which was also approaching the loop site. This is a slow wavefront, indicated by 'S' (19:20:12 UT), which slowly passed through the loop site (see images at 19:20:12 and 19:24:48 UT). Therefore, these images reveal the existence of both faster and slower coronal waves as they propagated towards the west from the flare site.

Figure 3 displays the selected base-difference images during the flare. We plot a larger field of view in these images in order to show the propagation of the faster wave from the solar disk to above the limb. The dome-like expansion of the faster wavefront ('F') can be seen in AIA 211 Å images. The faster ('F') and slower ('S') wavefronts can be seen simultaneously in the image at 19:20:07 UT. To show the propagation of the faster wavefront, we select a slice cut (indicated by 'B') in the plane of the sky along the wave propagation direction close to the western limb. The space–time plots of these two slices (A and B) are shown in Figure 4. The top panel shows the space–time plot of AIA 211 Å intensity distributions along slice 'A' (refer to image 19:15:12 UT in Figure 2). The top panel shows the propagating bright fast and slow wavefronts 'F' and 'S'. The coronal dimming behind these fronts is evident in these plots. We measured the distance–time of these two
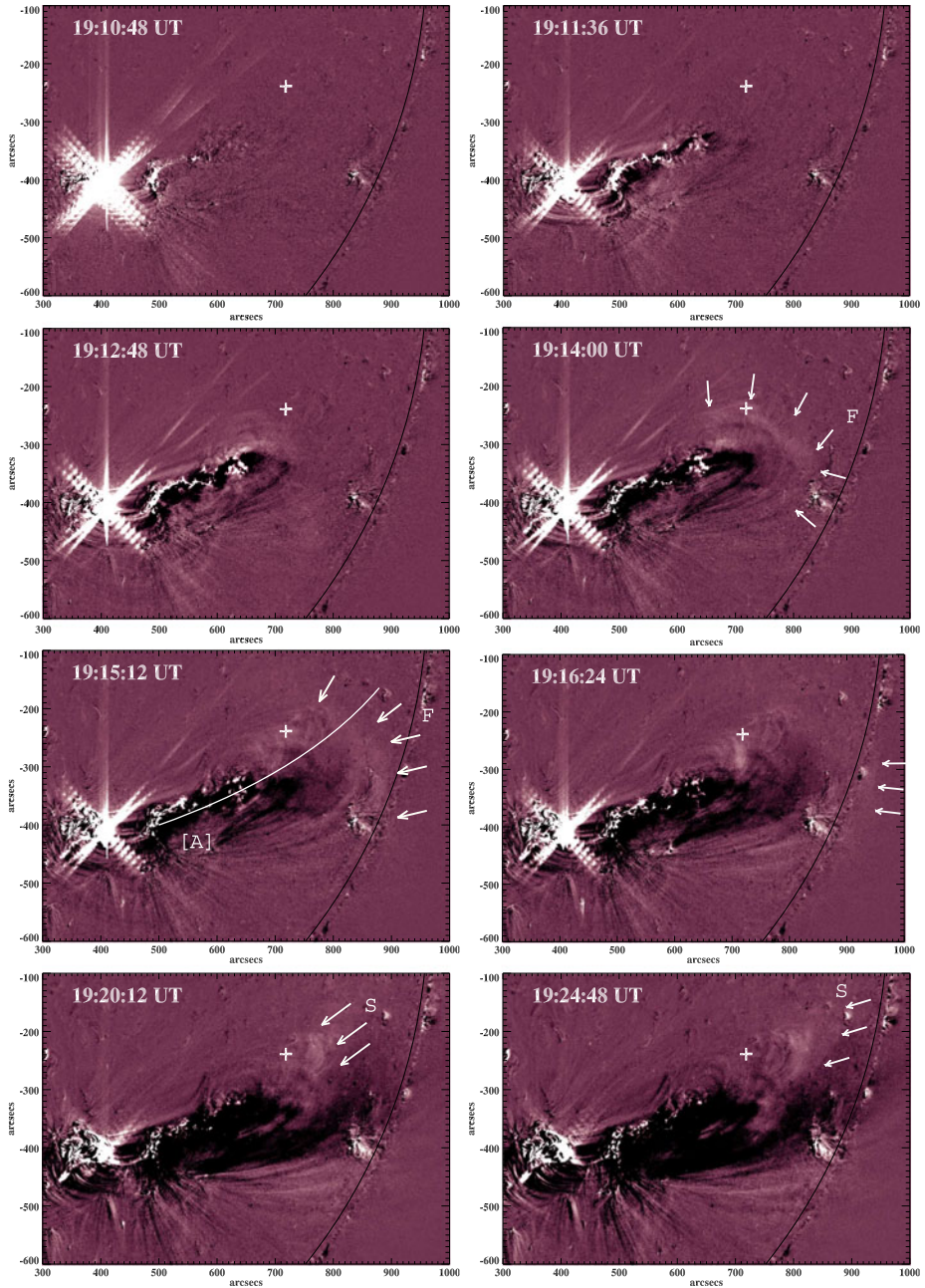
Figure 2 SDO/AIA EUV 211 Å base-difference images showing the propagation of coronal waves (indicated by arrows). The location of the oscillating coronal loop apex is indicated by the '+' symbol in each image. The loop started oscillating when the leading edge of the faster wave approached the loop system. White line 'A' shows the great circle along the solar surface in the direction of wave propagation. The faster and slower waves are indicated by 'F' and 'S', respectively.
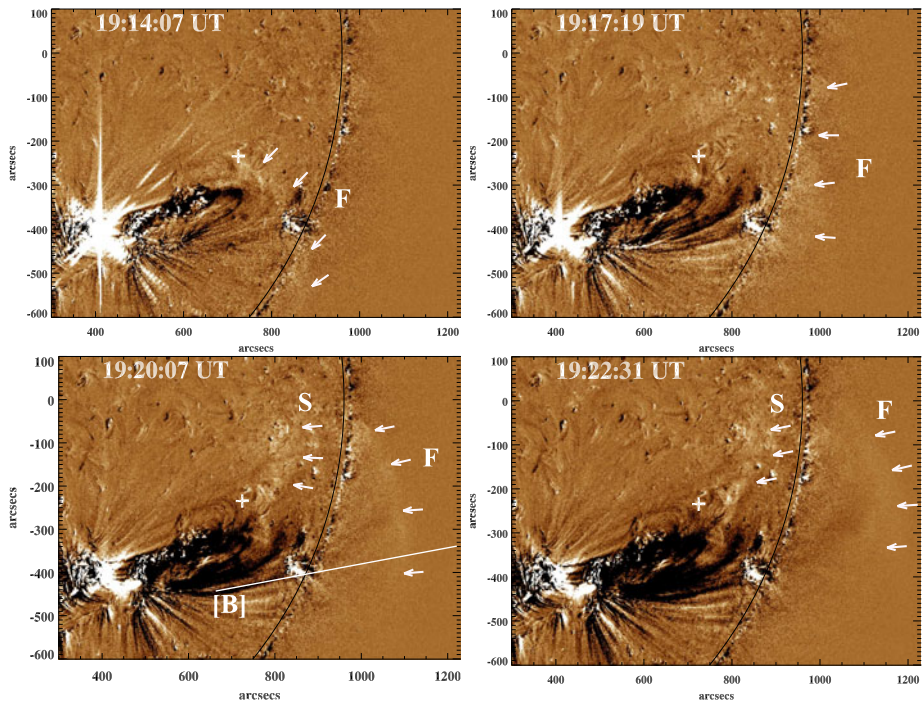
Figure 3 SDO/AIA EUV 193 Å base-difference images showing the propagation of coronal waves (indicated by the arrows). The location of the oscillating coronal loop apex is indicated by the '+' symbol in each image. The line marked by 'B' shows the slice cut along the direction of wave propagation. The faster and slower waves are indicated by 'F' and 'S', respectively.

propagating wavefronts using the top panel. The measured data points are indicated in the top panel by red (diamond) and blue (+) for faster and slower wave components. We apply a linear fit to these data points and attain the speeds of these waves, which are 1086 km s^{-1} and 276 km s^{-1}, respectively. The bottom panel shows the fast wave propagation along slice 'B' across the western limb. It shows a diffuse slower component (marked by '+'), which is the signature of the expanding CME loop.

However, we did not observe any filament or flux rope eruption in AIA EUV images during the flare event. A small loop eruption was observed from the flare site visible in high-cadence AIA 94 Å images (Paper I), which moved along the westward direction. The top panel of Figure 5 displays the selected AIA 193 Å running-difference images above the solar western limb across which the wave propagates. The first image at 19:20:07 UT shows the bright circular fast wavefront (indicated by arrows), marked by 'F'. In the next images, we roughly see the shock front straddling over the leading edge of the expanding CME loop. For investigating the CME that was associated with the M2.9 flare, we use LASCO C2 (*Large Angle Spectrometric Coronagraph*) white-light observations between $\approx 2 - 6 R_{\odot}$ (Brueckner *et al.*, 1995). The bottom panel of Figure 5 displays the white-light running-difference images, which are combined with co-temporal AIA 193 Å EUV running-difference images. These images show the CME propagation away from the western limb. The second image at 19:24:06 UT shows the expanding CME loop in the AIA field of view, and we see the bright blob-shaped CME structure. In the coronograph field of view, the CME speed measured from the linear fit is found to be 350 km s^{-1}, and it shows an acceleration of 47.5 m s^{-2} dur-
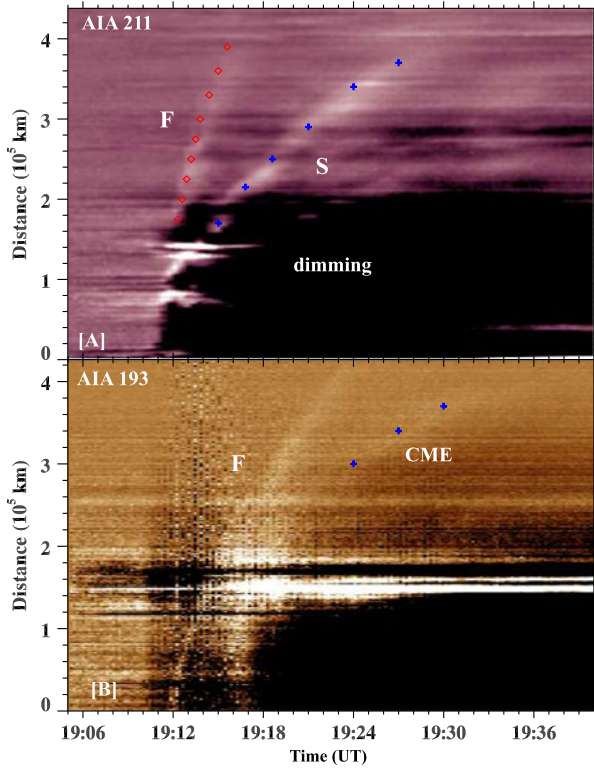
Figure 4 Temporal evolution of the 211 Å and 193 Å base-difference intensity distributions along slice 'A' (top) and slice 'B' (bottom), respectively. Faster and slower waves are marked by 'F' and 'S', respectively. The mean speeds (from the linear fit) of the faster and slower waves are, respectively, $\approx 1086\ \mathrm{km\,s^{-1}}$ and $\approx 276\ \mathrm{km\,s^{-1}}$.

ing the propagation. The fast shock disappeared in the LASCO field of view and we could observe only a blob-shaped structure in the CME (refer to image at 20:36:05 UT). This blob may be linked with the narrow coronal loop, which erupted along with the flare observed in AIA 94 Å images.

We used STEREO-A (*Solar TErrestrial RElations Observatory*, Kaiser *et al.*, 2008) EUV 195 Å images to see the coronal waves from a different viewing angle. The size of each image is 2048 × 2048 pixels with a 1.6″ per pixel sampling (Wuelser *et al.*, 2004). In STEREO-A, the active region was located close to the eastern limb. The top panel of Figure 6 shows the 195 Å EUV running-difference images, where we see a typical EIT wave. We can compare the direction of the EIT wave, which is the same as the slower one seen in the AIA 211 Å base-difference images. In order to estimate the speed of the EIT wave, we have visually tracked the position of the propagating wavefront along the great circle shown in Figure 6.

The inner coronagraph (COR1) of the *Sun Earth Connection Coronal and Heliospheric Investigation* (SECCHI, Howard *et al.*, 2008) instrument on board STEREO allows us to investigate the CME kinematics in the low corona from $1.4 – 4.0 R_{\odot}$ with a high time cadence of ≈ 5 or 10 min and a spatial resolution of 3.75″. We used COR1 observations to view the CME during the flare. The bottom panel of Figure 6 displays the base-difference images of
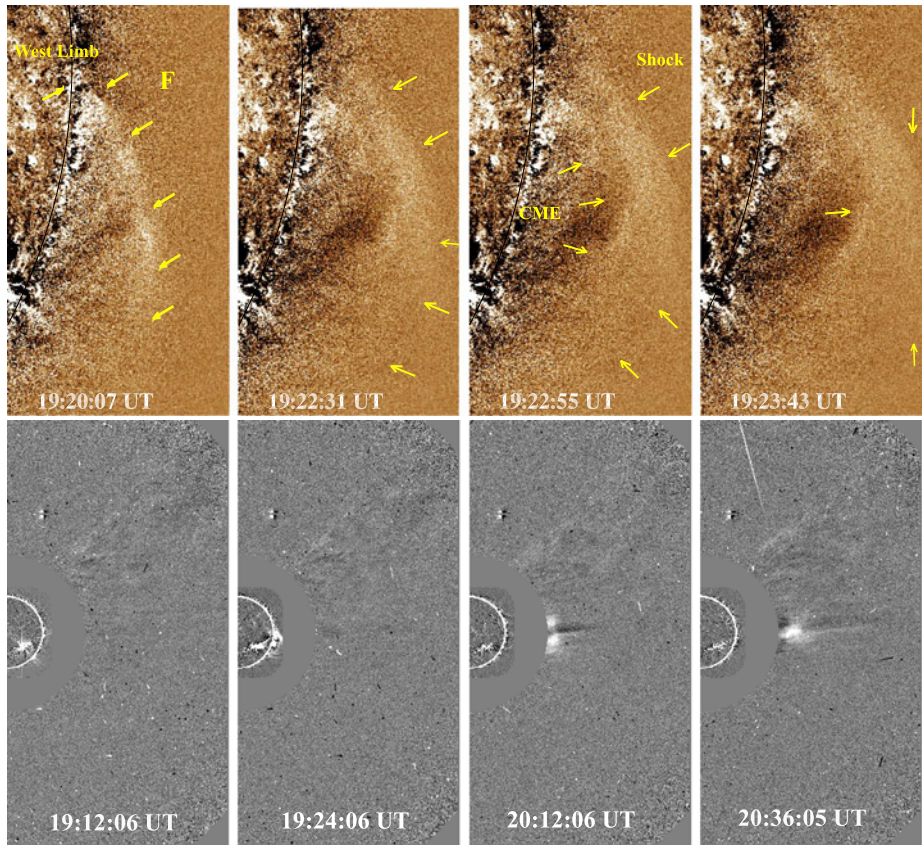
Figure 5 Top: AIA 193 Å base-difference images showing the propagating faster wavefront 'F' ahead of the expanding CME loop. The size of each image is $380'' \times 700''$. Bottom: AIA 193 Å and LASCO C2 composite difference images showing the CME associated with the flare with a speed ≈ 350 km s^{-1}.

the associated CME observed by COR1. These images also show a weak and slow CME, which was possibly associated with small loop eruption observed in AIA 94 Å images. The estimated speed of the CME from COR1 height–time measurements was ≈ 340 km s^{-1}, which is close to the CME speed measured by LASCO C2 (≈ 350 km s^{-1}).

The top panel of Figure 7 displays the dynamic radio spectrum in $25 - 180$ MHz observed at Sagamore Hill radio station, USA (Straka and Castelli, 1970). We can see the type III and metric type II radio bursts during the flare. The drifting stripes of metric type II emission (*i.e.* fundamental and second harmonic) are known as the signature of coronal shock waves, and radio emission frequencies can be converted to emission heights of the shock by adopting a coronal density model. We used the middle of the emission lane for the fundamental ($+$) and second harmonic ($*$) bands. We estimated the shock heights by using one-fold Newkirk coronal density model (Newkirk, 1961). The corresponding emission heights for both bands have been plotted in bottom panel of Figure 7, which shows the emission heights in between $1.3 - 1.5 R_\odot$ (from Sun center). Using the linear fit to the emission heights, we estimated the shock speed from fundamental and second harmonic, *i.e.* ≈ 800 km s^{-1} and 680 km s^{-1}, respectively. We also use the two-fold Newkirk coronal density model to estimate the uncertainty caused by a (provisional) choice of density model. The radio-source
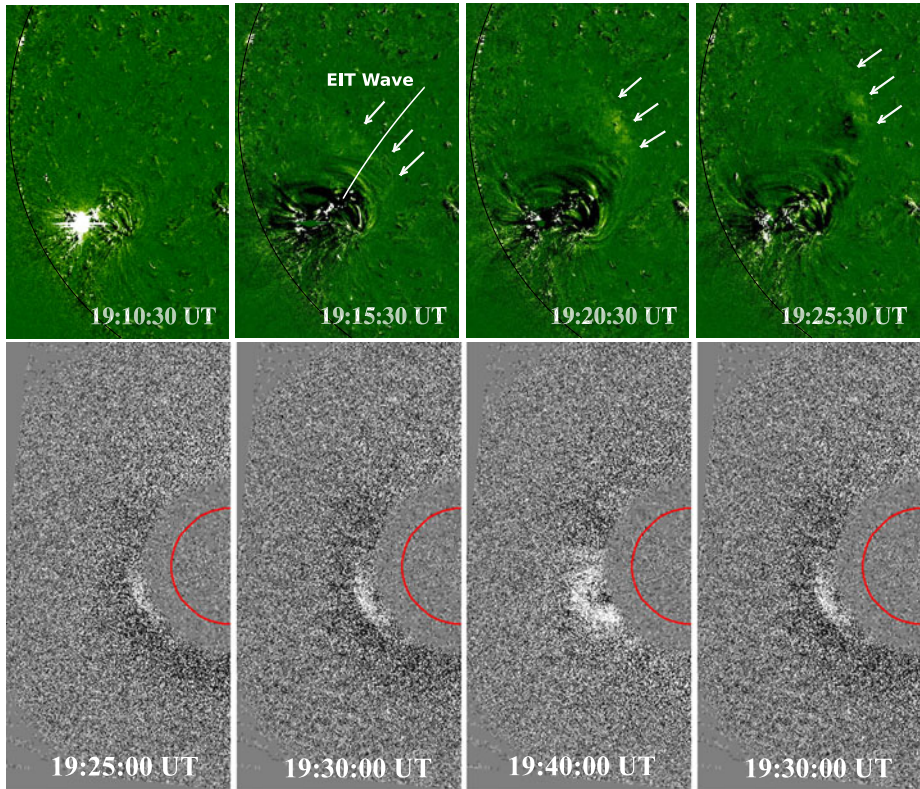
Figure 6 Top: STEREO-A EUV 195 Å running-difference images showing the flare, dimmings and the propagation of the EIT wave. The white line shows the great circle along the solar surface in the direction of wave propagation. Bottom: STEREO-A COR1 base-difference images showing a loop-like slow CME (speed $\approx 340 \text{ km s}^{-1}$).

heights estimated using this model are larger in comparison to the previous one (shown by red color). The mean speed of the shock from fundamental and second harmonic are *i.e.* $\approx 975 \text{ km s}^{-1}$ and 830 km s^{-1}, respectively. We also plotted the projected height of the plasmoid (diamond) measured in AIA 94 Å images and the mean speed of the plasmoid was found to be $\approx 1197 \text{ km s}^{-1}$. The plasmoid was observed nearly 3 min prior to the type II radio burst, which may be associated with the formation of a shock wave in the corona.

These measurements of the wave fronts' distance, along with the GOES soft X-ray (1 – 8 Å) flux, are plotted in the top panel of Figure 8. The 'circle' and 'plus' symbols correspond to the AIA 211 Å measurements, whereas the 'triangle' symbol corresponds to the STEREO 195 Å. We measured the position of the wave fronts 'F' and 'S' at different times using the AIA 211 Å slice 'A' in Figure 4. The position of the leading edge of the EIT wave shown in STEREO 195 Å images has been measured by drawing a great circle from the flare center (indicated in the top panel of Figure 6). The calculated speeds of these waves are plotted in the middle panel. For AIA observations, the speed of the faster wave decreases from ≈ 1390 to $\approx 830 \text{ km s}^{-1}$, whereas that of the slower wave decreases from ≈ 416 to $\approx 166 \text{ km s}^{-1}$. In STEREO, the speed of the EIT wave decreased from 320 to 254 km s^{-1}. The faster wave showed a significant deceleration within the first 5 min. The average deceleration of the faster wave is $\approx -2830 \text{ m s}^{-2}$, whereas $\approx -350 \text{ m s}^{-2}$ for the slower wave. Note that the
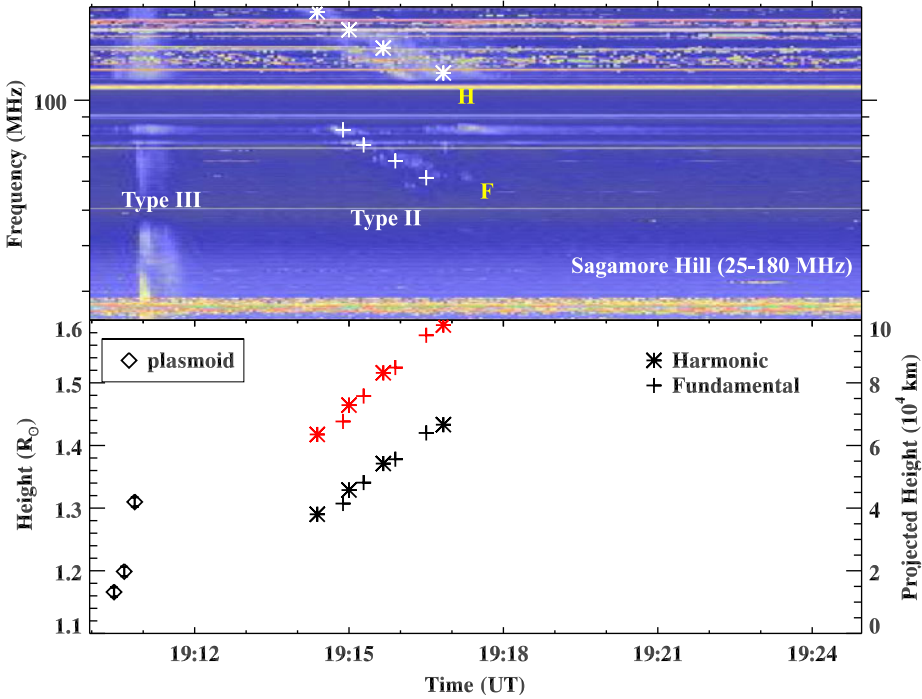
Figure 7 Top: The dynamic radio spectrum in 25 – 180 MHz observed at Sagamore Hill station on 16 October 2010, showing type III and type II radio bursts during the flare. Bottom: The source heights of type II burst inferred from the fundamental band (+) and harmonic band (∗) using Newkirk 1-fold (lower) and 2-fold (upper, red) density models, respectively. The scale for the projected height (*y*-axis) of the plasmoid (diamond) is given on the right side (note the different units).

uncertainty in the speed estimation is mainly due to the error in the distance measurement in AIA and STEREO, which is taken as four pixels (*i.e.* 2.4″ for AIA and 6.4″ for STEREO).

The difference in speed between the EIT wave in STEREO and the faster wave in AIA implies the existence of two coronal waves, a faster and a slower wave, which again confirms our result in Figure 4. The speed of the slower wave in AIA is comparable to that observed in STEREO. The faster wave was missed by STEREO. This is probably due to the low cadence of STEREO, which is not sufficient to detect the faster wave (Chen and Wu, 2011). Therefore, the EIT wave in STEREO is not cospatial with the fast coronal wave observed in AIA. The observational evidence of the coronal Moreton wave ahead of the EIT wave (using AIA data) was recently confirmed by Chen and Wu (2011). They found that the speed of the coronal Moreton wave was nearly three times higher than the EIT wave speed. The present observations also most likely reveal the existence of the fast-mode MHD coronal Moreton wave ahead of the EIT wave. In Figure 8, we also included the mean speed of the plasmoid (red diamond) and the mean speed of the coronal shock (star) measured from the drift rate of type II (fundamental band), which show a good correspondence between all the speeds.

In order to investigate the magnetic field environment of the active region, we used the potential field source surface (PFSS) extrapolation (Altschuler and Newkirk, 1969; Schatten, Wilcox, and Ness, 1969) before the flare event at 18:04 UT. Figure 9 shows the PFSS extrapolation of the active region. The flare site, the coronal wave, and the oscillating loop are indicated by arrows. Comparing the PFSS extrapolation with AIA 211 Å images
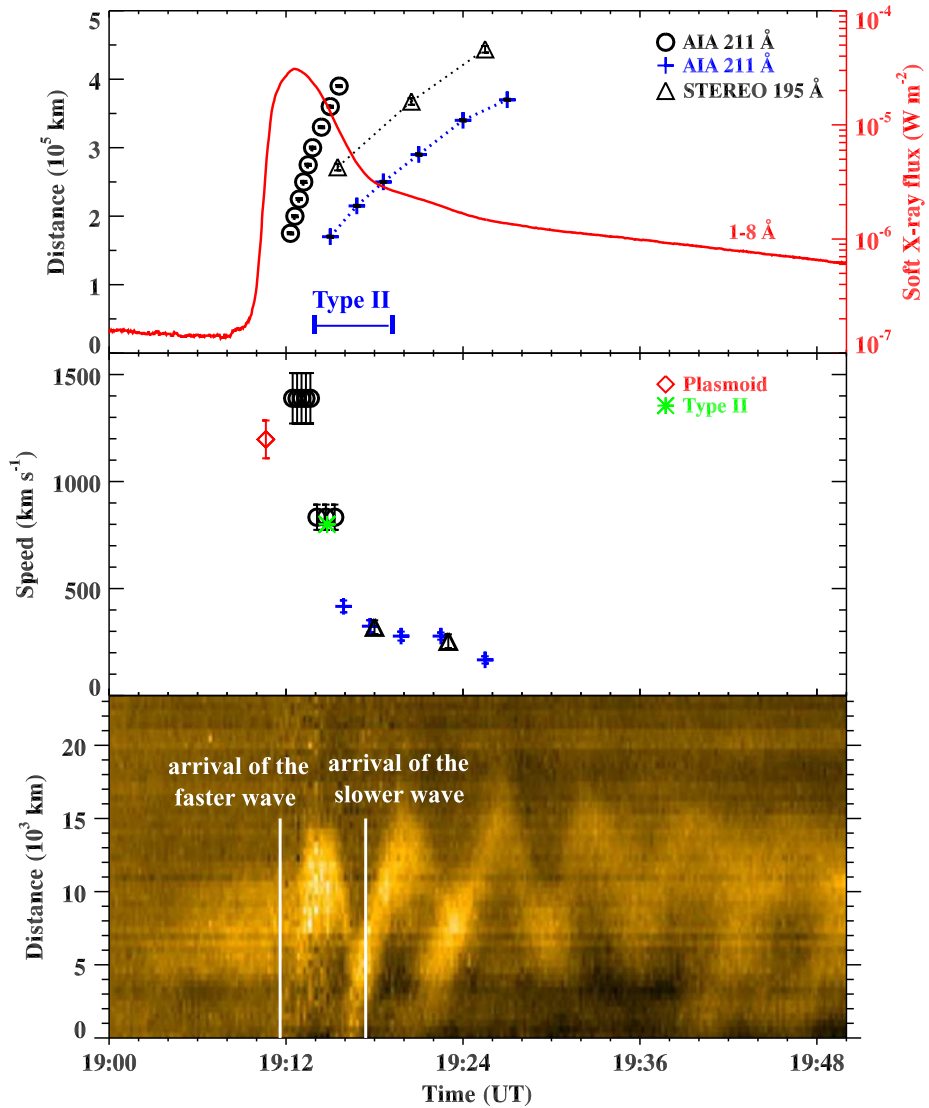
Figure 8 Top: Distance–time profiles of the coronal waves derived from AIA 211 (circle and plus symbols) and STEREO 195 Å (triangle) images. The GOES soft X-ray profile in 1 – 8 Å wavelength band is depicted as the red curve. The duration of the type II radio burst is marked by a blue horizontal line. Middle: Speed profiles for both faster and slower wave. The plasmoid speed (red diamond) and coronal shock speed derived from type II (star) radio burst have also been plotted. Bottom: Space–time plot of the oscillating loop along the slice cut shown in the left panel of Figure 10.

reveals that the field line above the flare site seems to be stretched during the wave propagation. Note that the lateral expansion of the wave/dimming (the direction from southwest to northeast) is negligible. It is probably because the magnetic field lines along the narrow corridor are closed inside the corridor rather than linking outside, and only these field lines responded to the CME eruption.
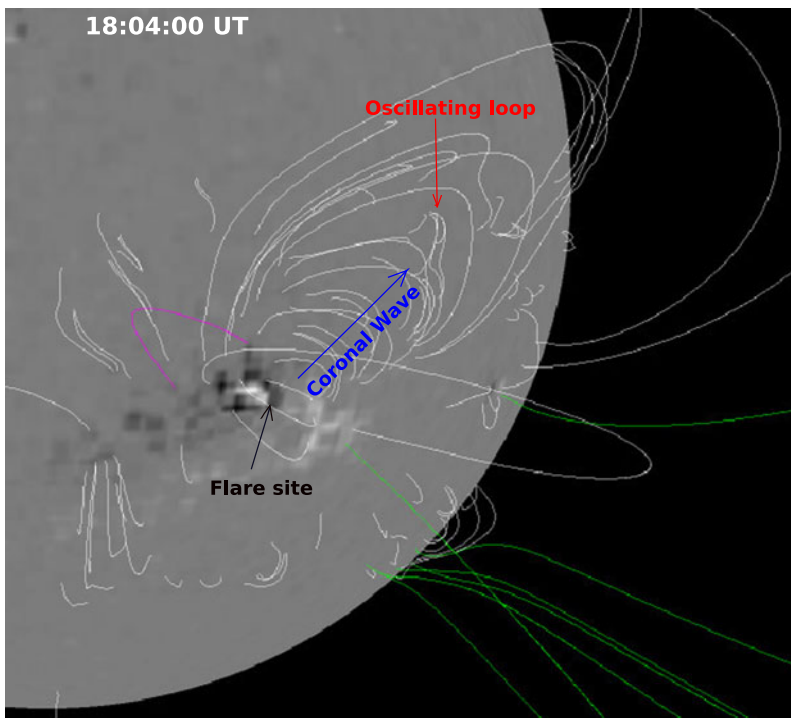
Figure 9 PFSS extrapolation of the active region NOAA 11112 at 18:04 UT on 16 October 2010.

2.2. Coronal Loop-Oscillation

The right panel of Figure 10 displays the AIA 211 Å EUV base-difference image at 19:14:00 UT in the enlarged view showing the wavefronts (indicated by arrows) of both fast and slow waves, which are marked, respectively, by 'F' and 'S'. The position of the loop apex is marked by the '+' symbol. This gives a clear indication of the successive interaction of the faster and slower waves with the coronal loop. The AIA 171 Å image in the left panel shows the position of the loop that presented transverse oscillations (indicated by the red arrow, and the online 171 Å movie) during the passage of coronal waves. The location of the slice cut for the space–time plot is marked as a white line in this image, and the space–time plot is presented in the lower panel of Figure 8.

The loop started oscillating when the leading front of the faster wave approached it (see aia171.avi, the online supplementary movie for loop oscillations). The space–time plot reveals that the amplitude of the oscillation of the selected thread shows an increase before a weak decay, which is very unusual for coronal loop oscillations (Aschwanden and Schrijver, 2011). The loop oscillation continued about five periods and the measured period of oscillation was 6.3 minutes. These measurements of the oscillation period of the loop strand match well with the findings of Aschwanden and Schrijver (2011). However, here our aim is to shed light on the most likely driver of the coronal loop oscillations. We mark the arrival times of the faster and slower waves to the coronal loop in the space–time plot, and it seems that the faster coronal wave is the first driver to generate the loop oscillations. In addition, type II radio burst was also observed at the time of coronal wave propagation towards west.
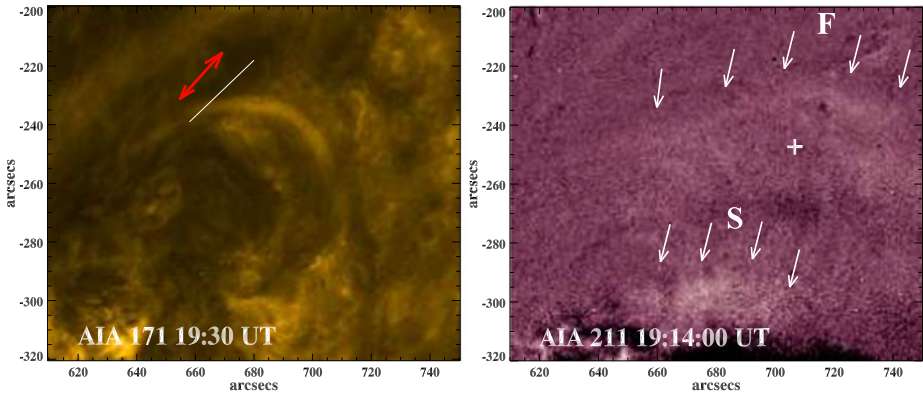
Figure 10 Left: AIA 171 Å EUV image showing the loop, which presented transverse oscillations (indicated by the red arrow) during the passage of coronal waves. The position of the slice cut for the space–time plot in Figure 8 is marked as the white line in the image. Right: AIA 211 Å EUV base-difference image showing the wavefronts (indicated by arrows) of both the faster and the slower wave, marked by 'F' and 'S', respectively. The position of the loop apex is marked by the '+' symbol.

The duration of type II is indicated by a horizontal line in the top panel of Figure 8. The arrival of a propagating faster wave, its relation with the flare, the metric type II radio burst, and the start of loop oscillation collectively indicate that the coronal loop started to oscillate due to its interaction with a coronal shock wave.

The peculiar behavior of this loop oscillation event is that the oscillation did not show strong decay as usual, but, instead, its amplitude was increasing in the first two periods. In this sense, it should be noted that the slower wave (EIT wave) passed through the location of coronal loop after the faster wave. The EIT wave arrived at the loop at about 19:16:24 UT (refer to Figure 8). Coincidentally, the amplitude of the oscillation increased after the arrival of the EIT wave (front S, see bottom panel of Figure 8). The increase of the loop oscillation was observed until the wave passed there. Later when it moved out, the oscillations decayed weakly. Therefore, it is likely that the passage of the slower wave caused the strengthening of loop oscillation for a longer time.

Eto *et al.* (2002) also have found that the filament winking was initiated by the passage of a Moreton wave, and was enhanced when the EIT wave passed the filament. In their study, the times of visibility for the Moreton wave did not overlap with those of the EIT wave. Instead, the continuation of the Moreton wave was implied by the filament oscillation. Using the position and speed measurements, they clearly showed that the Moreton wave differed physically from the EIT wave in their case. In our case, the loop oscillation behavior generated by the impact of the faster and the slower coronal waves are consistent with the filament oscillations initiated by the passage of the Moreton and EIT waves. Recently, Asai *et al.* (2012) have reported the first simultaneous observation of an Hα Moreton wave, the corresponding EUV fast coronal waves, and a slow and bright EIT wave. They also observed the filament/prominence oscillations when the wave approached it. However, we do not have Hα observations during the flare. But we see the propagating brightening/disturbance in AIA 304 Å images (corresponding to chromosphere and transition region) in a similar direction to the EUV wave, visible in AIA 211 and 193 Å images. Our observational findings are also consistent with Asai *et al.* (2012).

3. Discussion and Conclusions

We analyzed the multiwavelength observations of the M2.9/1N flare that occurred on 16 October 2010 from AR NOAA 11112. We first discussed the identification of two waves associated with the flare/CME event, *i.e.*, a faster coronal Moreton wave and a slower EIT wave. According to the SDO/AIA observations, the flare and the CME were associated with a faster and a slower waves, which moved towards the west, decelerating from ≈ 1390 to ≈ 830 km s^{-1} and from ≈ 416 to ≈ 166 km s^{-1}, respectively. In STEREO 195 Å only one diffuse EIT wave was discernable, decelerating from ≈ 320 to ≈ 254 km s^{-1}. The slower wave in SDO/AIA is interpreted as a classical EIT wave, consistent with the STEREO observations.

According to Uchida's Model (Uchida, 1968, 1970), the Moreton wave is a sweeping skirt on the chromosphere of the MHD fast-mode shock wave which propagates in the corona. Therefore, this model predicts the existence of a coronal counterpart of the chromospheric Moreton wave at the same place and with the same velocity as that of the Moreton wave. Thompson *et al.* (2000) reported that there are two components in EIT waves, *i.e.*, bright/sharp and diffuse EIT waves. The sharp EIT wave and Hα Moreton wave are cospatial, whereas the relationship between the diffuse EIT and Moreton wave was not clear. In the present event, we observed the diffuse EIT wave in STEREO 195 Å images, which was cospatial with the slower wave observed by SDO/AIA. Wu *et al.* (2001) and Warmuth *et al.* (2001) suggested that the diffuse EIT waves are decelerated Moreton waves, namely: not only sharp EIT waves but also diffuse EIT waves are coronal counterparts of the chromospheric Moreton waves. However, Eto *et al.* (2002) found that the diffuse EIT wave was not the coronal counterpart of the chromospheric Moreton wave in their analyzed event. In the present paper, we revealed the existence of both faster and slower wavefronts, which are not cospatial. In addition, they have very different velocities. The existence of these two waves is consistent with prediction by the Chen *et al.* (2002) model and it was confirmed by Harra and Sterling (2003) and Chen and Wu (2011).

A remote small coronal loop started to oscillate with a period of 6.3 minutes as the faster wave hit it. The detailed study of the loop oscillation has been presented by Aschwanden and Schrijver (2011). We suggest that the faster wave is most likely the first driver of loop oscillation, and the oscillation was enhanced by the ensuing EIT wave. PFSS extrapolation and the direction of the fast wavefront in association with a loop oscillation suggest that the coronal Moreton wave propagates across the closed magnetic loops. The visibility of the coronal Moreton wave may be related to the local magnetic field, and tends to be enhanced in weaker magnetic field (Uchida, 1970).

The initiation of a filament oscillation that preceded the arrival of the EIT wave in Eto *et al.* (2002) was suggested as evidence in support of the idea that EIT waves are not coronal Moreton waves. On the other hand, Warmuth *et al.* (2004b) interpreted this event in terms of a tilted coronal wavefront: since the filament is located higher up, the more tenuous upper – and thus less observable – parts of the wavefront will reach it first. Furthermore, determining at which time the filament actually begins to oscillate can lead to quite ambiguous results, so that the possible errors might be much larger than the errors on the wavefronts (Warmuth, 2010). But, in the present case, we have shown that the triggering of loop oscillation is at the arrival of the faster wavefront, and that the oscillation was enhanced with the passage of the slower wavefront, *i.e.* the EIT wave.

A metric type II burst was also observed during the propagation of the coronal waves. The speed of the shock wave derived from type II frequency drift rate (≈ 800 km s^{-1}) matches well with the speed of the faster coronal wave associated with the flare/CME. The type II

radio burst may be associated with the high speed coronal wave as it moves nearly with Alfvénic speed in the corona. The observed faster coronal wave is probably the fast-mode coronal Moreton wave, and the presence of type II during this time supports the presence of a fast-mode MHD shock wave as predicted by Uchida (1974). We found good temporal, spatial correspondence and matching speeds between EUV coronal Moreton wave and the shock wave derived from type II radio burst.

In a statistical analysis of the coronal loop oscillations observed by TRACE, Hudson and Warmuth (2004) showed the strong association of TRACE loop oscillation events with type II bursts, indicating that some of them were directly caused by blast waves. In their observations, only certain loops oscillate, whereas other nearby loops remain stationary, which was consistent with the highly directional nature of blast waves (Smith and Harvey, 1971; Warmuth *et al.*, 2004a). On the other hand, a piston-driven-type shock could be launched by ejecta with a smaller scale (*e.g.*, sprays or ejecta observed with the *Yokhoh* soft X-ray telescope instead of an initial pressure pulse. For example, Klein *et al.* (1999) have shown an X-ray blob (projected speed ≈ 770 km s^{-1}) as a plausible driver of a fast shock in the corona. They could act as a temporary piston, and either they could generate a perturbation that then steepens into a shock, or there could be a short phase of a driven shock, after which the shock propagates freely (Warmuth *et al.*, 2004b; Veronig *et al.*, 2010; Muhr *et al.*, 2011). In the present case, we observe (in AIA 94 Å images) a high speed plasmoid (projected speed ≈ 1197 km s^{-1}) moving away from the flare site during the flare impulsive phase (Paper I) and this eruption may be responsible for driving the high speed shock and type II burst observed in this event. This favors the scenario of the piston-driven shock.

Recently, Warmuth and Mann (2011) analyzed a large sample of 176 EIT wave events and, based on their kinematical behavior, they found evidence for three distinct populations of coronal EUV waves: initially fast waves ($v \geq 320$ km s^{-1}) that show pronounced deceleration (class 1 events), then waves with moderate ($v \approx 170 - 320$ km s^{-1}) and nearly constant speeds (class 2), and finally slow waves ($v \leq 130$ km s^{-1}) showing a rather erratic behavior (class 3). They explained classes 1 and 2 in terms of the fast-mode wave/shock model, whereas class 3 events were explained to be due to magnetic reconfiguration. By combining data from AIA and EIS, Harra *et al.* (2011) and Veronig *et al.* (2011) examined a coronal wave and found that the main wave front travels at ≈ 500 km s^{-1} and is strongly redshifted (*i.e.*, as the wave propagates it also pushes plasma downward with a speed of ≈ 20 km s^{-1}). They concluded that the observed wave was generated by the outgoing CME, as in the scenario for the classic Moreton wave (*i.e.* fast MHD wave), which pushes down the chromospheric plasma along the shock front.

Our observations reveal the signature of a fast coronal Moreton wave and associated loop oscillation that was initiated by the wave. On the other hand, the slower wave observed in this event cannot be the top part of the CME leading loop, since it impacted the small coronal loop. It could be associated with the leg of the CME leading loop, while EIT wave was already found to be cospatial with the CME leg (Chen, 2009; Dai *et al.*, 2010). Therefore, we conclude that the slower wave is the classical EIT wave.

In conclusion, we presented the multiwavelength observations of both the faster and slower coronal waves, which may be the first and the second drivers of the oscillations of a remote loop. Using high spatial and temporal data from space and ground-based instruments, further studies should be performed in order to shed more light on the flare processes and their association with large-scale coronal waves.

References

Altschuler, M.D., Newkirk, G.: 1969, Magnetic fields and the structure of the solar corona. I: Methods of calculating coronal fields. *Solar Phys.* **9**, 131 – 149. doi:10.1007/BF00145734.

Asai, A., Ishii, T.T., Isobe, H., Kitai, R., Ichimoto, K., UeNo, S., Nagata, S., Morita, S., Nishida, K., Shiota, D., Oi, A., Akioka, M., Shibata, K.: 2012, First simultaneous observation of an Hα Moreton wave, EUV wave, and filament/prominence oscillations. *Astrophys. J. Lett.* **745**, L18. doi:10.1088/2041-8205/745/2/L18.

Aschwanden, M.J., Schrijver, C.J.: 2011, Coronal loop oscillations observed with Atmospheric Imaging Assembly-Kink mode with cross-sectional and density oscillations. *Astrophys. J.* **736**, 102. doi:10.1088/0004-637X/736/2/102.

Attrill, G.D.R.: 2010, Dispelling illusions of reflection: A new analysis of the 2007 May 19 coronal "wave" event. *Astrophys. J.* **718**, 494 – 501. doi:10.1088/0004-637X/718/1/494.

Biesecker, D.A., Myers, D.C., Thompson, B.J., Hammer, D.M., Vourlidas, A.: 2002, Solar phenomena associated with "EIT Waves". *Astrophys. J.* **569**, 1009 – 1015. doi:10.1086/339402.

Brueckner, G.E., Howard, R.A., Koomen, M.J., Korendyke, C.M., Michels, D.J., Moses, J.D., Socker, D.G., Dere, K.P., Lamy, P.L., Llebaria, A., Bout, M.V., Schwenn, R., Simnett, G.M., Bedford, D.K., Eyles, C.J.: 1995, The Large Angle Spectroscopic Coronagraph (LASCO). *Solar Phys.* **162**, 357 – 402. doi:10.1007/BF00733434.

Chen, P.F.: 2006, The relation between EIT waves and solar flares. *Astrophys. J. Lett.* **641**, L153 – L156. doi:10.1086/503868.

Chen, P.F.: 2009, The relation between EIT waves and coronal mass ejections. *Astrophys. J. Lett.* **698**, L112 – L115. doi:10.1088/0004-637X/698/2/L112.

Chen, P.F.: 2011, Coronal mass ejections: Models and their observational basis. *Living Rev. Solar Phys.* **8**, 1.

Chen, P.F., Fang, C.: 2011, "EIT waves" and coronal mass ejections. In: Choudhuri, A.R., Banerjee, D. (eds.) *ASI* **CS-2**, 229 – 239.

Chen, P.F., Fang, C., Shibata, K.: 2005, A full view of EIT waves. *Astrophys. J.* **622**, 1202 – 1210. doi:10.1086/428084.

Chen, P.F., Wu, Y.: 2011, First evidence of coexisting EIT wave and coronal Moreton wave from SDO/AIA observations. *Astrophys. J. Lett.* **732**, L20. doi:10.1088/2041-8205/732/2/L20.

Chen, P.F., Wu, S.T., Shibata, K., Fang, C.: 2002, Evidence of EIT and Moreton waves in numerical simulations. *Astrophys. J. Lett.* **572**, L99 – L102. doi:10.1086/341486.

Cho, K.S., Bong, S.C., Moon, Y.J., Shanmugaraju, A., Kwon, R.Y., Park, Y.D.: 2011, Relationship between multiple type II solar radio bursts and CME observed by STEREO/SECCHI. *Astron. Astrophys.* **530**, A16. doi:10.1051/0004-6361/201015578.

Cliver, E.W., Laurenza, M., Storini, M., Thompson, B.J.: 2005, On the origins of solar EIT waves. *Astrophys. J.* **631**, 604 – 611. doi:10.1086/432250.

Dai, Y., Auchère, F., Vial, J.C., Tang, Y.H., Zong, W.G.: 2010, Large-scale extreme-ultraviolet disturbances associated with a limb coronal mass ejection. *Astrophys. J.* **708**, 913 – 919. doi:10.1088/0004-637X/708/2/913.

Delaboudinière, J.P., Artzner, G.E., Brunaud, J., Gabriel, A.H., Hochedez, J.F., Millier, F., Song, X.Y., Au, B., Dere, K.P., Howard, R.A., Kreplin, R., Michels, D.J., Moses, J.D., Defise, J.M., Jamar, C., Rochus, P., Chauvineau, J.P., Marioge, J.P., Catura, R.C., Lemen, J.R., Shing, L., Stern, R.A., Gurman, J.B., Neupert, W.M., Maucherat, A., Clette, F., Cugnon, P., van Dessel, E.L.: 1995, EIT: Extreme-Ultraviolet Imaging telescope for the SOHO mission. *Solar Phys.* **162**, 291 – 312. doi:10.1007/BF00733432.

Delannée, C., Aulanier, G.: 1999, CME associated with transequatorial loops and a bald patch flare. *Solar Phys.* **190**, 107 – 129. doi:10.1023/A:1005249416605.

Eto, S., Isobe, H., Narukage, N., Asai, A., Morimoto, T., Thompson, B., Yashiro, S., Wang, T., Kitai, R., Kurokawa, H., Shibata, K.: 2002, Relation between a Moreton wave and an EIT wave observed on 1997 November 4. *Publ. Astron. Soc. Japan* **54**, 481 – 491.

Gallagher, P.T., Long, D.M.: 2011, Large-scale bright fronts in the solar corona: A review of "EIT waves". *Space Sci. Rev.* **158**, 365 – 396. doi:10.1007/s11214-010-9710-7.

Harra, L.K., Sterling, A.C.: 2003, Imaging and spectroscopic investigations of a solar coronal wave: Properties of the wave front and associated erupting material. *Astrophys. J.* **587**, 429 – 438. doi:10.1086/368079.

Harra, L.K., Sterling, A.C., Gömöry, P., Veronig, A.: 2011, Spectroscopic observations of a coronal Moreton wave. *Astrophys. J. Lett.* **737**, L4. doi:10.1088/2041-8205/737/1/L4.

Howard, R.A., Moses, J.D., Vourlidas, A., Newmark, J.S., Socker, D.G., Plunkett, S.P., Korendyke, C.M., Cook, J.W., Hurley, A., Davila, J.M., Thompson, W.T., St Cyr, O.C., Mentzell, E., Mehalick, K., Lemen, J.R., Wuelser, J.P., Duncan, D.W., Tarbell, T.D., Wolfson, C.J., Moore, A., Harrison, R.A., Waltham, N.R., Lang, J., Davis, C.J., Eyles, C.J., Mapson-Menard, H., Simnett, G.M., Halain, J.P., Defise, J.M., Mazy, E., Rochus, P., Mercier, R., Ravet, M.F., Delmotte, F., Auchere, F., Delaboudiniere, J.P., Bothmer, V., Deutsch, W., Wang, D., Rich, N., Cooper, S., Stephens, V., Maahs, G., Baugh, R., McMullin, D., Carter, T.: 2008, Sun Earth Connection Coronal and Heliospheric Investigation (SECCHI). *Space Sci. Rev.* **136**, 67 – 115. doi:10.1007/s11214-008-9341-4.

Hudson, H.S., Warmuth, A.: 2004, Coronal loop oscillations and flare shock waves. *Astrophys. J. Lett.* **614**, L85 – L88. doi:10.1086/425314.

Hudson, H.S., Khan, J.I., Lemen, J.R., Nitta, N.V., Uchida, Y.: 2003, Soft X-ray observation of a large-scale coronal wave and its exciter. *Solar Phys.* **212**, 121 – 149. doi:10.1023/A:1022904125479.

Kaiser, M.L., Kucera, T.A., Davila, J.M., St. Cyr, O.C., Guhathakurta, M., Christian, E.: 2008, The STEREO mission: An introduction. *Space Sci. Rev.* **136**, 5 – 16. doi:10.1007/s11214-007-9277-0.

Khan, J.I., Aurass, H.: 2002, X-ray observations of a large-scale solar coronal shock wave. *Astron. Astrophys.* **383**, 1018 – 1031. doi:10.1051/0004-6361:20011707.

Kienreich, I.W., Temmer, M., Veronig, A.M.: 2009, STEREO quadrature observations of the three-dimensional structure and driver of a global coronal wave. *Astrophys. J. Lett.* **703**, L118 – L122. doi:10.1088/0004-637X/703/2/L118.

Kienreich, I.W., Veronig, A.M., Muhr, N., Temmer, M., Vršnak, B., Nitta, N.: 2011, Case study of four homologous large-scale coronal waves observed on 2010 April 28 and 29. *Astrophys. J. Lett.* **727**, L43. doi:10.1088/2041-8205/727/2/L43.

Klassen, A., Pohjolainen, S., Klein, K.L.: 2003, Type II radio precursor and X-ray flare emission. *Solar Phys.* **218**, 197 – 210. doi:10.1023/B:SOLA.0000013034.61996.c4.

Klassen, A., Karlický, M., Aurass, H., Jiřička, K.: 1999, On two distinct shocks during the flare of 9 July 1996. *Solar Phys.* **188**, 141 – 154.

Klassen, A., Aurass, H., Mann, G., Thompson, B.J.: 2000, Catalogue of the 1997 SOHO-EIT coronal transient waves and associated type II radio burst spectra. *Astron. Astrophys. Suppl. Ser.* **141**, 357 – 369. doi:10.1051/aas:2000125.

Klein, K.L., Khan, J.I., Vilmer, N., Delouis, J.M., Aurass, H.: 1999, X-ray and radio evidence on the origin of a coronal shock wave. *Astron. Astrophys.* **346**, 53 – 56.

Kumar, P., Park, S.-H., Cho, K.-S., Bong, S.-C.: 2012, Multiwavelength study of a solar eruption from AR NOAA 11112 I. Flux emergence, sunspot rotation and triggering of a solar flare. *Solar Phys.* accepted. arXiv:1210.3413. ADS:2012arXiv1210.3413K.

Lemen, J.R., Title, A.M., Akin, D.J., Boerner, P.F., Chou, C., Drake, J.F., Duncan, D.W., Edwards, C.G., Friedlaender, F.M., Heyman, G.F., Hurlburt, N.E., Katz, N.L., Kushner, G.D., Levay, M., Lindgren, R.W., Mathur, D.P., McFeaters, E.L., Mitchell, S., Rehse, R.A., Schrijver, C.J., Springer, L.A., Stern, R.A., Tarbell, T.D., Wuelser, J.P., Wolfson, C.J., Yanari, C., Bookbinder, J.A., Cheimets, P.N., Caldwell, D., Deluca, E.E., Gates, R., Golub, L., Park, S., Podgorski, W.A., Bush, R.I., Scherrer, P.H., Gummin, M.A., Smith, P., Auker, G., Jerram, P., Pool, P., Soufli, R., Windt, D.L., Beardsley, S., Clapp, M., Lang, J., Waltham, N.: 2012, The Atmospheric Imaging Assembly (AIA) on the Solar Dynamics Observatory (SDO). *Solar Phys.* **275**, 17 – 40. doi:10.1007/s11207-011-9776-8.

Magara, T., Chen, P., Shibata, K., Yokoyama, T.: 2000, A unified model of coronal mass ejection-related type II radio bursts. *Astrophys. J. Lett.* **538**, L175 – L178. doi:10.1086/312813.

Magdalenić, J., Vršnak, B., Pohjolainen, S., Temmer, M., Aurass, H., Lehtinen, N.J.: 2008, A flare-generated shock during a coronal mass ejection on 24 December 1996. *Solar Phys.* **253**, 305 – 317. doi:10.1007/s11207-008-9220-x.

Magdalenić, J., Marqué, C., Zhukov, A.N., Vršnak, B., Žic, T.: 2010, Origin of coronal shock waves associated with slow coronal mass ejections. *Astrophys. J.* **718**, 266 – 278. doi:10.1088/0004-637X/718/1/266.

Moreton, G.E., Ramsey, H.E.: 1960, Recent observations of dynamical phenomena associated with solar flares. *Publ. Astron. Soc. Pac.* **72**, 357. doi:10.1086/127549.

Muhr, N., Vršnak, B., Temmer, M., Veronig, A.M., Magdalenić, J.: 2010, Analysis of a global Moreton wave observed on 2003 October 28. *Astrophys. J.* **708**, 1639 – 1649. doi:10.1088/0004-637X/708/2/1639.

Muhr, N., Veronig, A.M., Kienreich, I.W., Temmer, M., Vršnak, B.: 2011, Analysis of characteristic parameters of large-scale coronal waves observed by the Solar-Terrestrial Relations Observatory/Extreme Ultraviolet Imager. *Astrophys. J.* **739**, 89. doi:10.1088/0004-637X/739/2/89.

Narukage, N., Hudson, H.S., Morimoto, T., Akiyama, S., Kitai, R., Kurokawa, H., Shibata, K.: 2002, Simultaneous observation of a Moreton wave on 1997 November 3 in Hα and soft X-rays. *Astrophys. J. Lett.* **572**, L109 – L112. doi:10.1086/341599.

Newkirk, G. Jr.: 1961, The solar corona in active regions and the thermal origin of the slowly varying component of solar radio radiation. *Astrophys. J.* **133**, 983 – 1013. doi:10.1086/147104.

Patsourakos, S., Vourlidas, A.: 2009, "Extreme Ultraviolet Waves" are waves: First quadrature observations of an extreme ultraviolet wave from STEREO. *Astrophys. J. Lett.* **700**, L182 – L186. doi:10.1088/0004-637X/700/2/L182.

Patsourakos, S., Vourlidas, A., Wang, Y.M., Stenborg, G., Thernisien, A.: 2009, What is the nature of EUV waves? First STEREO 3D observations and comparison with theoretical models. *Solar Phys.* **259**, 49 – 71. doi:10.1007/s11207-009-9386-x.

Pesnell, W.D., Thompson, B.J., Chamberlin, P.C.: 2012, The Solar Dynamics Observatory (SDO). *Solar Phys.* **275**, 3 – 15. doi:10.1007/s11207-011-9841-3.

Schatten, K.H., Wilcox, J.M., Ness, N.F.: 1969, A model of interplanetary and coronal magnetic fields. *Solar Phys.* **6**, 442 – 455. doi:10.1007/BF00146478.

Schou, J., Scherrer, P.H., Bush, R.I., Wachter, R., Couvidat, S., Rabello-Soares, M.C., Bogart, R.S., Hoeksema, J.T., Liu, Y., Duvall, T.L., Akin, D.J., Allard, B.A., Miles, J.W., Rairden, R., Shine, R.A., Tarbell, T.D., Title, A.M., Wolfson, C.J., Elmore, D.F., Norton, A.A., Tomczyk, S.: 2012, Design and ground calibration of the Helioseismic and Magnetic Imager (HMI) instrument on the Solar Dynamics Observatory (SDO). *Solar Phys.* **275**, 229 – 259. doi:10.1007/s11207-011-9842-2.

Smith, S.F., Harvey, K.L.: 1971, Observational effects of flare-associated waves. In: Macris, C.J. (ed.) *Physics of the Solar Corona*, Astrophys. Space Sci. Lib. **27**, 156.

Straka, R.M., Castelli, J.P.: 1970, Observations at the Sagamore Hill solar radio observatory. *Nature* **226**, 1149 – 1152. doi:10.1038/2261149a0.

Thompson, B.J., Plunkett, S.P., Gurman, J.B., Newmark, J.S., St. Cyr, O.C., Michels, D.J.: 1998, SOHO/EIT observations of an Earth-directed coronal mass ejection on May 12, 1997. *Geophys. Res. Lett.* **25**, 2465 – 2468. doi:10.1029/98GL50429.

Thompson, B.J., Gurman, J.B., Neupert, W.M., Newmark, J.S., Delaboudinière, J.P., St. Cyr, O.C., Stezelberger, S., Dere, K.P., Howard, R.A., Michels, D.J.: 1999, SOHO/EIT observations of the 1997 April 7 coronal transient: Possible evidence of coronal Moreton waves. *Astrophys. J. Lett.* **517**, L151 – L154. doi:10.1086/312030.

Thompson, B.J., Reynolds, B., Aurass, H., Gopalswamy, N., Gurman, J.B., Hudson, H.S., Martin, S.F., St. Cyr, O.C.: 2000, Observations of the 24 September 1997 coronal flare waves. *Solar Phys.* **193**, 161 – 180.

Uchida, Y.: 1968, Propagation of hydromagnetic disturbances in the solar corona and Moreton's wave phenomenon. *Solar Phys.* **4**, 30 – 44. doi:10.1007/BF00146996.

Uchida, Y.: 1970, Diagnosis of coronal magnetic structure by flare-associated hydromagnetic disturbances. *Publ. Astron. Soc. Japan* **22**, 341.

Uchida, Y.: 1974, Behavior of the flare produced coronal MHD wavefront and the occurrence of type II radio bursts. *Solar Phys.* **39**, 431 – 449. doi:10.1007/BF00162436.

Veronig, A.M., Temmer, M., Vršnak, B.: 2008, High-cadence observations of a global coronal wave by STEREO EUVI. *Astrophys. J. Lett.* **681**, L113 – L116. doi:10.1086/590493.

Veronig, A.M., Temmer, M., Vršnak, B., Thalmann, J.K.: 2006, Interaction of a Moreton/EIT wave and a coronal hole. *Astrophys. J.* **647**, 1466 – 1471. doi:10.1086/505456.

Veronig, A.M., Muhr, N., Kienreich, I.W., Temmer, M., Vršnak, B.: 2010, First observations of a dome-shaped large-scale coronal extreme-ultraviolet wave. *Astrophys. J. Lett.* **716**, L57 – L62. doi:10.1088/2041-8205/716/1/L57.

Veronig, A.M., Gomory, P., Kienreich, I.W., Muhr, N., Vršnak, B., Temmer, M., Warren, H.P.: 2011, Plasma diagnostics of an EIT wave observed by Hinode/EIS and SDO/AIA. *Astrophys. J. Lett.* **743**, L10.

Vršnak, B., Cliver, E.W.: 2008, Origin of coronal shock waves: Invited review. *Solar Phys.* **253**, 215 – 235. doi:10.1007/s11207-008-9241-5.

Vršnak, B., Lulić, S.: 2000a, Formation of coronal MHD shock waves – I. The basic mechanism. *Solar Phys.* **196**, 157 – 180.

Vršnak, B., Lulić, S.: 2000b, Formation of coronal MHD shock waves – II. The pressure pulse mechanism. *Solar Phys.* **196**, 181 – 197.

Vršnak, B., Ruždjak, V., Zlobec, P., Aurass, H.: 1995, Ignition of MHD shocks associated with solar flares. *Solar Phys.* **158**, 331 – 351. doi:10.1007/BF00795667.

Vršnak, B., Warmuth, A., Brajša, R., Hanslmeier, A.: 2002, Flare waves observed in Helium I 10 830 Å. A link between Hα Moreton and EIT waves. *Astron. Astrophys.* **394**, 299 – 310. doi:10.1051/0004-6361:20021121.

Wang, Y.M.: 2000, EIT waves and fast-mode propagation in the solar corona. *Astrophys. J. Lett.* **543**, L89 – L93. doi:10.1086/318178.

Warmuth, A.: 2007, Large-scale waves and shocks in the solar corona. In: Klein, K.-L., MacKinnon, A.L. (eds.) *Lecture Notes in Physics* **725**, Springer, Berlin, 107.

Warmuth, A.: 2010, Large-scale waves in the solar corona: The continuing debate. *Adv. Space Res.* **45**, 527 – 536. doi:10.1016/j.asr.2009.08.022.

Warmuth, A., Mann, G.: 2011, Kinematical evidence for physically different classes of large-scale coronal EUV waves. *Astron. Astrophys.* **532**, A151. doi:10.1051/0004-6361/201116685.

Warmuth, A., Mann, G., Aurass, H.: 2005, First soft X-ray observations of global coronal waves with the GOES solar X-ray Imager. *Astrophys. J. Lett.* **626**, L121 – L124. doi:10.1086/431756.

Warmuth, A., Vršnak, B., Aurass, H., Hanslmeier, A.: 2001, Evolution of two EIT/Hα Moreton waves. *Astrophys. J. Lett.* **560**, L105 – L109. doi:10.1086/324055.

Warmuth, A., Vršnak, B., Magdalenić, J., Hanslmeier, A., Otruba, W.: 2004a, A multiwavelength study of solar flare waves. I. Observations and basic properties. *Astron. Astrophys.* **418**, 1101 – 1115. doi:10.1051/0004-6361:20034332.

Warmuth, A., Vršnak, B., Magdalenić, J., Hanslmeier, A., Otruba, W.: 2004b, A multiwavelength study of solar flare waves. II. Perturbation characteristics and physical interpretation. *Astron. Astrophys.* **418**, 1117 – 1129. doi:10.1051/0004-6361:20034333.

Wills-Davey, M.J., Attrill, G.D.R.: 2009, EIT Waves: A changing understanding over a solar cycle. *Space Sci. Rev.* **149**, 325 – 353. doi:10.1007/s11214-009-9612-8.

Wu, S.T., Zheng, H., Wang, S., Thompson, B.J., Plunkett, S.P., Zhao, X.P., Dryer, M.: 2001, Three-dimensional numerical simulation of MHD waves observed by the Extreme Ultraviolet Imaging Telescope. *J. Geophys. Res.* **106**, 25089 – 25102. doi:10.1029/2000JA000447.

Wuelser, J.P., Lemen, J.R., Tarbell, T.D., Wolfson, C.J., Cannon, J.C., Carpenter, B.A., Duncan, D.W., Gradwohl, G.S., Meyer, S.B., Moore, A.S., Navarro, R.L., Pearson, J.D., Rossi, G.R., Springer, L.A., Howard, R.A., Moses, J.D., Newmark, J.S., Delaboudiniere, J.P., Artzner, G.E., Auchere, F., Bougnet, M., Bouyries, P., Bridou, F., Clotaire, J.Y., Colas, G., Delmotte, F., Jerome, A., Lamare, M., Mercier, R., Mullot, M., Ravet, M.F., Song, X., Bothmer, V., Deutsch, W.: 2004, EUVI: the STEREO-SECCHI extreme ultraviolet imager. In: Fineschi, S., Gummin, M.A. (eds.) *SPIE* **CS-5171**, 111 – 122. doi:10.1117/12.506877.

Zhukov, A.N.: 2011, EIT wave observations and modeling in the STEREO era. *J. Atmos. Solar-Terr. Phys.* **73**, 1096 – 1116. doi:10.1016/j.jastp.2010.11.030.